Magnetic phase diagram and critical behavior of electron-doped $La_xCa_{1-x}MnO_3$ ($0 \leqslant x \leqslant 0.25$) nanoparticles

Yang Wang and Hong Jin Fan

Division of Physics and Applied Physics, School of Physical and Mathematical Sciences, Nanyang Technological University, 21 Nanyang Link, 637371, Singapore

(Received 14 February 2011; revised manuscript received 10 May 2011; published 21 June 2011)

A comparative study of electron-doped perovskite manganites $La_xCa_{1-x}MnO_3$ ($0 \leqslant x \leqslant 0.25$) in nanoparticle and bulk form is reported. The bulks and nanoparticles exhibit different magnetic evolutions. Overall with increasing x, the bulks have a phase-separated ground state with ferromagnetic (FM) clusters and antiferromagnetic (AFM) matrix coexisting. The FM clusters gradually grow, and the magnetization M peaks at $x = 0.1$. Subsequently, charge-ordering (CO) or local CO occurs, which suppresses the increase in FM clusters but favors the development of antiferromagnetism so M starts to decrease. Finally the system becomes a homogeneous AFM state at $x > 0.18$. For the nanoparticles in the range of $0 \leqslant x \leqslant 0.1$, the ground state is similar to that of the bulks, but M is slightly increased because of a surface ferromagnetism. Nevertheless because of the structure distortion induced by surface pressure and the size effect, CO does not occur in the nanoparticles. Consequently, the ferromagnetism still gradually develops at $x > 0.1$ and thus M monotonously rises. M reaches a maximum at $x = 0.18$, after which the competition between ferromagnetism and antiferromagnetism induces a cluster-glass (CG) state. On the basis of these observations the phase diagrams for both bulks and nanoparticles are established. For the nanoparticles that display enhanced ferromagnetism the critical behavior analysis indicates that they fall into a three-dimensional (3D) Heisenberg ferromagnet class.

DOI: 10.1103/PhysRevB.83.224409 PACS number(s): 75.47.Lx, 75.75.Fk, 61.46.Df

I. INTRODUCTION

Compared with conventional bulks nanosized materials may exhibit many novel properties, so nanomaterials such as nanoparticles, nanowires, and nanocomposites are currently a focus of investigations. A typical example is the recent attention on nanosized perovskite manganites with the $R_xA_{1-x}MnO_3$ formula (where R and A are rare earth and alkaline earth, respectively).[1–15] Although the transport properties, along with magnetic-phase diagrams, in these manganites have been widely studied for decades, the unusual magnetic behaviors in the $R_xA_{1-x}MnO_3$ nanostructures attract intense new attention. For example, charge-ordering (CO) state and antiferromagnetism are highly stable in half-doped manganites (e.g., $La_{0.5}Ca_{0.5}MnO_3$ and $Pr_{0.5}Ca_{0.5}MnO_3$), but they are significantly suppressed with reducing grain size down to nanometer scale accompanied by an enhanced ferromagnetism.[1–6] Similar phenomena are also observed in hole-doped manganites with antiferromagnetic (AFM) CO ground state.[7–10] There also exists size-dependent exchange-bias effect and glassy behaviors in these nanostructures.[9,11–13] The suppression of CO, along with the enhanced ferromagnetism in the nanosized manganites, is primarily explained by the size effect and surface effect.[1–7,10,14] Theoretically, Monte Carlo calculation and phenomenological models also show an enhancement of surface-charge density and validate a suppression of CO-AFM phase and an emergence of ferromagnetic (FM) order near the surface.[16,17] Such surface magnetism inevitably existing in nanoparticles/nanowires will drastically influence the magnetic properties and vary the superexchange interactions at surface, which allows a formation of FM shells and therefore results in a natural FM/AFM interface and exchange bias effect.[12,13,16,17]

Although nanostructured manganites with various sizes and morphologies have been researched, almost all studies primarily focus only on the magnetism differences between the nanostructures and bulks as well as size-dependent magnetic behaviors at a fixed component. Systematic investigations on magnetic properties of $R_{1-x}A_xMnO_3$ nanostructures in a wide doping range are extremely scant; however, the evolutions of magnetic properties clearly reveal that such investigations are essential. In addition most investigations concern hole-doped and half-doped manganites (i.e., $x \geqslant 0.5$), whereas they pay less attention to electron-doped range (i.e., $x < 0.5$). In fact electron-doped manganites exhibit many special phenomena, and the phase diagrams of manganites in electron-doped and hole-doped ranges are pronouncedly asymmetrical because of the intrinsic differences of the ground-state characteristics.[18–20] The ground state of $R_xA_{1-x}MnO_3$ manganites is quite complex. The distinct ground states such as FM metal, charge-ordered insulator, or paramagnetic (PM) polaron liquid are especially energetically close because the interactions of different types in manganites are usually of comparable strength.[21] Consequently the ground state of a manganite can be of different types depending on which of the interactions win over, and thus the ground state is very sensitive to crystalline structure, carrier concentration, electric/magnetic field, and hydrostatic/chemical pressure, etc. Hence, the present-phase diagrams of $R_xA_{1-x}MnO_3$ manganites will be noticeably changed as the systems become nanosized.

In this paper we report a systematical study on the magnetic properties of electron-doped $La_xCa_{1-x}MnO_3$ nanoparticles in the range of $0 \leqslant x \leqslant 0.25$ and compare them with the bulk counterparts. Different from hole doping, electron-doped manganites never have purely FM-ground states; they exhibit magnetic-phase separated-ground state (coexistence of FM clusters and AFM matrix in the case of light electron doping) or charge-ordered AFM-ground state (in the case of heavy

electron doping).[18,22–24] However, in the nanosized electron-doped $La_xCa_{1-x}MnO_3$, we find that charge-ordered AFM phases do not appear. Instead, ferromagnetism gradually increases with La doping, and subsequently the system displays a glassy behavior, which is in strong contrast to the bulk counterparts. On the basis of these observations we have established a phase diagram for the $La_xCa_{1-x}MnO_3$ nanoparticles and further discussed the critical behavior and FM class in detail.

II. EXPERIMENTAL DETAILS

The $La_xCa_{1-x}MnO_3$ ($0 \leqslant x \leqslant 0.25$) nanoparticles and ceramic bulks were synthesized using a sol-gel method and a solid-state reaction, respectively. In the synthesis of nanoparticles, stoichiometric nitrates of lanthanum, calcium, and manganese were used as starting materials. First they were dissolved in deionized water to obtain a clear solution. Then an equal amount of ethylene glycol was added to the solution with stirring. The resultant mixed solution was heated on a hot plate up to 90 °C until a homogeneous gel was obtained. Subsequently the gel precursor was decomposed in a furnace at 250 °C to get precursor powders. Finally the black precursor powders were sintered at 600 °C for 2–3 h, and then crystalline nanoparticles were obtained. In the synthesis of ceramic bulks La_2O_3, $CaCO_3$, and MnO_2 powders were used as reagents; the detailed synthesis process is reported in Wang *et al.*[25]

Sample morphology was observed by a scanning electron microscopy (SEM, JEOL JSM-6700F). The SEM measurements indicate that the sizes of nanoparticles are in the range of 20–30 nm (see Fig. 1, insets), which are much smaller than the grain size (~3–5 μm) of the ceramic bulks.[25] Energy-dispersive spectroscopy analysis confirmed the composition and homogeneous distribution of the constituent elements, and the approximate oxygen content was ~2.99–3.00 for all samples. The chemical composition and oxygen content of the samples were further checked by iodometric titration and x-ray photoelectron spectroscopy (ESCA 100-VSW) analysis, which show that the oxygen content is stoichiometric "O_3" and the Mn^{3+}/Mn^{4+} ratio is correct. The results from the three parallel experiments are consistent, so the chemical composition of all samples is identical with the nominal $La_xCa_{1-x}MnO_3$. Therefore, although the magnetic properties of nanosized manganites could be influenced by changes in the Mn valence and oxygen nonstoichiometry,[26] herein these influences are negligible.

The phase purity and crystal structure were characterized by x-ray powder diffraction (XRD, MXPAHF-18 kW, MAC Science) analysis. The XRD results confirmed that all samples are a single phase of an orthorhombic perovskite structure (see Fig. 1). The structure parameters were determined by a Rietveld refinement, which reveal that the nanoparticles have a unit cell contraction of ~1.5%–2% compared with the bulk counterparts. As an example, the lattice parameters a, b, and c of $La_{0.18}Ca_{0.82}MnO_3$ bulk are 5.3336, 7.5322, and 5.3391 Å, but those of $La_{0.18}Ca_{0.82}MnO_3$ nanoparticles are 5.2829, 7.4576, and 5.3373 Å. Such unit-cell contraction has been observed in several mix-valent nanosized manganites and attributed to the surface pressure effect.[4,5,8] Magnetic properties of samples were measured by a magnetic-property measurement system (Quantum Design).

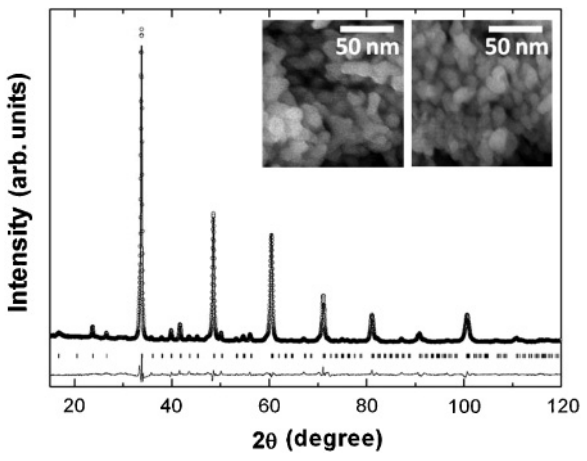

FIG. 1. XRD result and Rietveld-refinement pattern based on an orthorhombic *Pnma* space group for $La_{0.18}Ca_{0.82}MnO_3$ nanoparticles at $T = 300$ K. The observed data points are indicated with open circles, while the calculated pattern is shown as a continuous line. The positions of the reflections are indicated with vertical lines. The insets show the SEM images of $La_{0.18}Ca_{0.82}MnO_3$ (left) and $La_{0.1}Ca_{0.9}MnO_3$ (right) nanoparticles.

III. RESULTS AND DISCUSSION

The field-cooled (FC) magnetization M curves for all samples are shown in Fig. 2. The different magnetic behaviors between the nanoparticles and bulks are clear. The

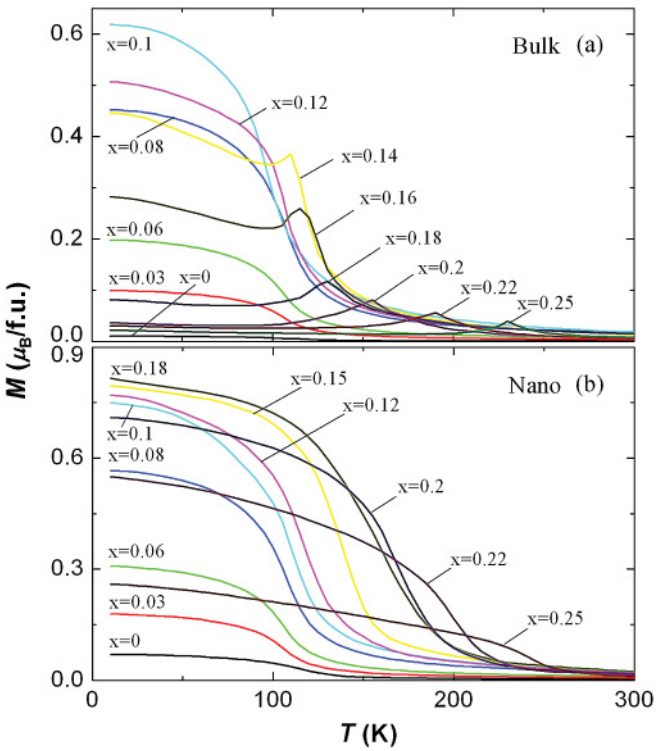

FIG. 2. (Color online) FC magnetizations for the samples under $H = 5$ T.

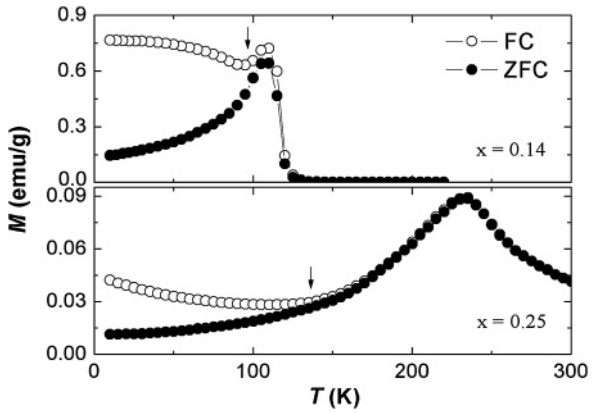

FIG. 3. FC (open symbols) and ZFC (closed symbols) magnetizations for the $x = 0.14$ and $x = 0.25$ bulks under a field of 100 Oe. The arrows indicate the bifurcation temperature of FC and ZFC curves that correspond to T_N.

magnetic evolution of $La_xCa_{1-x}MnO_3$ bulks is consistent with previously reported results of electron-doped $CaMnO_3$.[18,22,27] For the bulks, undoped $CaMnO_3$ is an AFM-band insulator with $T_N \sim 120$ K.[28] With La doping, the low-temperature M gradually rises because of the appearance of FM clusters, and M reached a maximum at $x = 0.1$; however, with further increasing La content, M begins to decrease and meanwhile a peak emerges in the $M(T)$ curves, which results from the formation of CO (or local CO) that suppresses the development of ferromagnetism. Finally the system becomes a homogeneous CO-AFM phase with heavier doping ($x > 0.18$).[18] The low-field magnetization measurements also manifest the CO-AFM characteristic in the heavily doped samples (see Fig. 3). The peak and the bifurcation in the dc FC and zero-field-cooling (ZFC) magnetizations correspond to the CO appearance and the AFM transition, respectively, and both CO temperature T_{CO} and AFM-transition temperature T_N increase with doping. In contrast the $La_xCa_{1-x}MnO_3$ nanoparticles exhibit another magnetic evolution. In the range of $0 \leqslant x \leqslant 0.1$ the $M(T)$ curves are approximately the same as those of $La_xCa_{1-x}MnO_3$ bulks, but the M values are somewhat higher than those of the bulks. This means that in this doping range the nanoparticles and bulks have identical intrinsic magnetic behaviors, whereas the additional M enhancement in nanoparticles should originate from a surface ferromagnetism.[14,16,17] It is interesting that although the M values rise with x in both bulks and nanoparticles, their difference, ΔM, nearly increases linearly [see Fig. 4(a) and 4(b)]. This suggests that the nanoparticles have increasing surface ferromagnetism with the development of FM clusters. On the basis of the core-shell model,[14,29] the deviation of the shell spins from a collinear AFM arrangement leads to uncompensated surface spins, which weakens the AFM interaction across the shell and thus causes ferromagnetism. Accordingly, increasing inside FM clusters will induce more surface spins to arrange with the core-FM ordering. Such correlation happens easier in the nanoparticles because of the rather small particle size. As a result, the nanoparticles show an additional ferromagnetism enhancement. Besides, in this doping range, the characteristic of an AFM matrix is still observable despite a clear ferromagnetism. As shown in

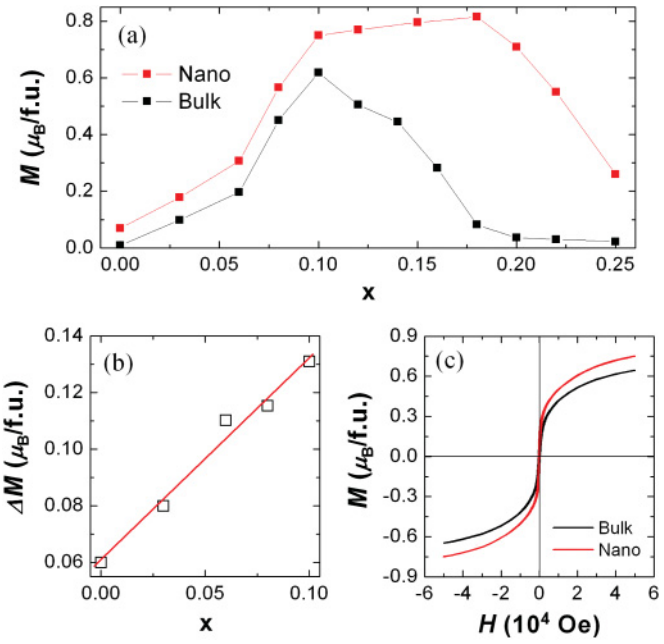

FIG. 4. (Color online) (a) Doping level x dependence of the magnetization at 5 K and 5 T for both bulks and nanoparticles. (b) Magnetization difference ΔM between the bulks and nanoparticles at 5 K and 5 T; the solid line is linear fitting. (c) M-H curves for the $La_{0.1}Ca_{0.9}MnO_3$ bulk and nanoparticle samples at 5 K.

Fig. 4(c), the M-H curves of both $La_{0.1}Ca_{0.9}MnO_3$ bulks and nanoparticles are not saturated even under a field of 5 T.

As x increases from $x = 0.1$, M in the nanoparticles remains increasing until $x = 0.18$, which happens instead of a decrease as observed in the bulks (Fig. 2). The magnetic-transition temperature T_C gradually increases with La doping. Meanwhile there are not any peaks in the $M(T)$ curves. These observations reveal an inherent difference between the nanoparticles and bulks, viz. in the nanoparticles CO is not established and FM clusters continue their development. Such phenomena are similar to the case observed in half-doped manganite nanostructures,[1,2,4,6] in which CO state is significantly suppressed and ferromagnetism is enhanced. The intrinsic origin of the suppression of CO still needs further study. Herein we propose the following reasons resulting in the breaking of CO. The surface pressure attributable to the small size in nanoparticles will create an effective hydrostatic pressure, which can cause not only the contraction of a unit cell but also structural distortions and strains deviating from the bulks. As suggested by Sarkar *et al.*,[4] such effective hydrostatic pressure induced by size reduction can freeze in the room-temperature structure, and thus the room-temperature structural distortions and/or stains in nanoparticles may not evolve with temperature, unlike the bulks. Table I lists the orthorhombic strains $O_{S\parallel}$ and $O_{S\perp}$ for two representative samples at different temperatures. Here both $O_{S\parallel}$ and $O_{S\perp}$ are driven by the intrinsic orthorhombic distortions, in which $O_{S\parallel} = 2(c-a)/(c+a)$ denotes the strain in an ac plane and $O_{S\perp} = 2(a+c-b\sqrt{2})/(a+c+b\sqrt{2})$ denotes the strain along the b axis. It is clear from Table I that in the bulk $O_{S\perp}$ is always larger than $O_{S\parallel}$, and $O_{S\perp}$ is noticeably enhanced below T_{CO}. In contrast, although the room-temperature $O_{S\parallel}$ and $O_{S\perp}$

TABLE I. Orthorhombic strains $O_{S\parallel}$ and $O_{S\perp}$ at different temperatures in the $La_{0.18}Ca_{0.82}MnO_3$ and $La_{0.25}Ca_{0.75}MnO_3$ samples.

	$La_{0.18}Ca_{0.82}MnO_3$				$La_{0.25}Ca_{0.75}MnO_3$			
	300 K	200 K	100 K	20 K	300 K	200 K	100 K	20 K
$O_{S\parallel}$(bulk)	0.001 03	0.001 47	0.001 71	0.001 31	0.001 26	0.001 12	0.001 51	0.001 89
$O_{S\perp}$(bulk)	0.001 93	0.003 90	0.011 56	0.014 82	0.002 61	0.002 98	0.017 29	0.021 55
$O_{S\parallel}$(nano)	0.010 24	0.010 32	0.009 76	0.009 80	0.012 23	0.011 57	0.013 40	0.012 95
$O_{S\perp}$(nano)	0.006 95	0.007 29	0.006 81	0.006 99	0.010 87	0.011 24	0.012 19	0.009 36

are increased in the nanoparticles because of surface pressure, both of them are nearly temperature independent, especially in the nanoparticles $O_{S\perp} < O_{S\parallel}$ in the whole temperature range. This should be an important reason leading to the absence of CO in the nanoparticles because the onset of CO needs a particular type of structural distortion to support it, and $O_{S\perp} > O_{S\parallel}$ is necessary for a CO to set in. Another reason concerns supercell modulation. In charge-ordered manganites the development of CO needs creation of a modulated superstructure and the periodicity of a supercell should be ~100 nm.[30] Therefore in our nanoparticles with a particle size of ~20–30 nm, CO cannot develop. In addition the surface disorder may also play a role in the suppression of CO transition. CO in manganites is achieved by an incommensurate configuration associated by the movement of extended CO-planar defects.[30,31] In the nanoparticles the disproportions are pinned at the surface hindering their movement, and the surface disorder can extend to a few layers into the interior of particles, which thus prevent the establishment of long-range CO state. On the other hand, short-range FM interactions in manganites are actually already present in the PM state because of thermally activated spin fluctuations.[32] In the case of a CO state CO suppresses the development of ferromagnetism: these FM correlations change to AFM correlations at T_{CO} and subsequently the system becomes AFM ordered at T_N. In the present nanoparticles, because of the absence of CO, the FM interactions progressively develop with decreasing temperature so that M continuously increases, as observed.

For the $La_xCa_{1-x}MnO_3$ nanoparticles where $x > 0.18$, M starts to decrease, but the $M(T)$ curves still display an FM-like characteristic, and T_C further increases [see Fig. 2(b)]. In this doping range CO remains absent because the conditions needed for CO to set in are still not met [also, no CO peak is observed in the $M(T)$ curves]. This implies that the FM clusters still exist, but the ferromagnetism is suppressed by factors other than CO. It should be mentioned here that our observations are somewhat different from the magnetic properties of $La_{0.2}Ca_{0.8}MnO_3$ nanocrystals reported by Markovich *et al.*[13] In their investigations although orbital ordering (OO) or CO are suppressed,[13,33] they do not disappear completely; that is, a weak OO/CO transition peak can be observed. We speculate that the different preparation method is responsible for this difference because in a different preparation process, as a consequence of different reaction dynamics, the crystalline structure distortions and strains of samples will be dissimilar, which could be crucial for the magnetic properties. The structure distortions and strains in Markovich *et al.*'s nanoparticles prepared by a glycine-nitrate method may be different from those in our nanoparticles prepared by a sol-gel method, and thus the conditions needed for CO or OO to set in are met in their nanoparticles; therefore, their $La_{0.2}Ca_{0.8}MnO_3$ nanoparticles of similar size exhibit a clear CO/OO-AFM characteristic and have much smaller magnetization than our $La_{0.2}Ca_{0.8}MnO_3$ nanoparticles. Another proof is the different magnetic phenomena observed in the $Ca_{0.82}La_{0.18}MnO_3$ nanowires (AFM with CO) and nanoparticles (FM-like without CO).[34] The nanowires and nanoparticles are prepared by different methods and have dissimilar structure distortions and strains; therefore, they exhibit different magnetic properties. On the other hand in Huang *et al.*'s report,[12] the $La_{0.25}Ca_{0.75}MnO_3$ nanoparticles are prepared by the same sol-gel method we used, and all of the $La_{0.25}Ca_{0.75}MnO_3$ nanoparticles exhibit quite similar magnetic behaviors (enhanced ferromagnetism, suppressed CO, and nearly same magnetization). Therefore it can be concluded that structural distortions/strains in the nanocrystal manganites, which is closely related to the preparation process, could be intrinsic and dominant in factors in determining whether CO is suppressed and ferromagnetism is developed.

To clarify the origin of the observed magnetic variations in these nanoparticles, the dc FC and ZFC magnetization, as well as ac susceptibility, are measured, as shown in Figs. 5 and 6. For all samples the FC and ZFC $M(T)$ curves split off below a certain temperature, indicating the onset of weak ferromagnetism.[11] Particularly, the shapes of the FC and ZFC $M(T)$ curves in these nanoparticles are similar to those in the manganite systems with FM cluster and AFM matrix coexisting,[35] and the irreversibility temperature T_{irr} at which the $M_{FC}(T)$ and $M_{ZFC}(T)$ diverge does not depend on applied magnetic field. This implies that FM clusters exist in all these nanoparticles. However, the ZFC $M(T)$ curves of the samples with $x > 0.18$ present some other noticeable features. The ZFC $M(T)$ curves exhibit an inflexion at a temperature lower than T_{irr}, after which M_{ZFC} obviously decreases [see Figs. 5(d)–5(f)]. Such phenomena are reminiscent of spin glass (SG) or cluster glass (CG). The ac-susceptibility measurements confirm their glassy behavior. As shown in Fig. 6, the inflexion temperature in the $M_{ZFC}(T)$ curves, denoted by T_f, is clearly frequency dependent. Therefore, we associate T_f with the freezing temperature of glass. The fitting-by-critical-slowing-down model shows that the fitting parameters fall in the range of CG instead of conventional SG. This is understandable because of the existence of FM clusters. Accordingly we conclude that the systems ($x > 0.18$) undergo a re-entrant CG state below T_f.

In the frame of the core-shell model an individual nanoparticle consists of an AFM-ordered core and FM-like shell, which may exhibit glass-like features.[5,14,15,17] Although the

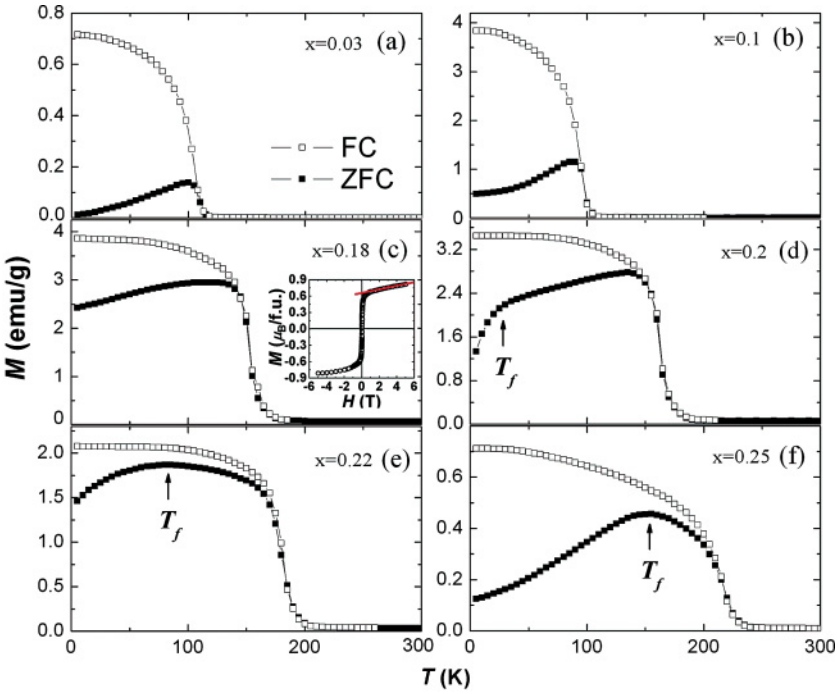

FIG. 5. (Color online) FC (open symbols) and ZFC (closed symbols) magnetizations for the $La_xCa_{1-x}MnO_3$ nanoparticles with different La content under a field of 1000 Oe. The arrows indicate the freezing temperature T_f. The inset of (c) shows the M-H curve at 5 K for the $x = 0.18$ nanoparticles; the red line denotes the extrapolation.

nature of the surface-shell contribution remains unclear,[36] in general the thickness of the surface layer with incommensurate magnetic structure increases as particle size decreases and as core-magnetic correlation rises.[11,37,38] Actually, there exists a delicate interplay as well as energy balance between the core and surface shell. According to the Heisenberg exchange theory, the exchange energy E_{ex} between two neighboring spins is given by

$$E_{ex} \propto -J_{ex} \sum_{i,j} S_i S_j \cos\theta_{ij}, \quad (1)$$

where J_{ex} is the exchange integral, and S_i and S_j are the spin-quantum number of spin i and j. For nanoparticles most core spins can be considered as antiparallel, i.e., $\theta_{ij} \approx 180^\circ$, but the FM-correlated-shell spins cause a higher E_{ex} across the shell. Such energy enhancement, together with the surface strain, leads to a large surface energy, which will hinder the development of inner FM clusters and FM coupling.[14]

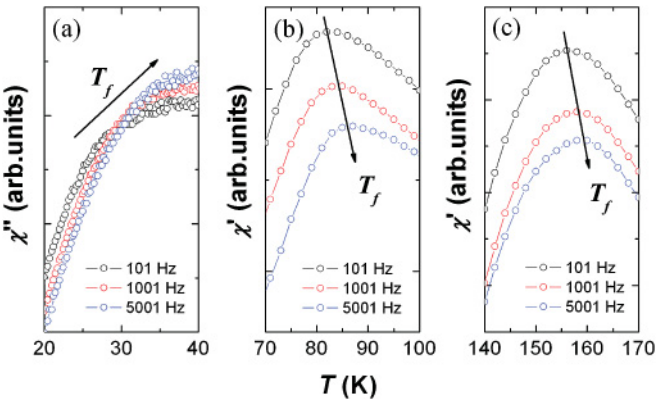

FIG. 6. (Color online) Temperature dependence of ac susceptibility of (a) $x = 0.2$, (b) $x = 0.22$, and (c) $x = 0.25$ nanoparticles at different frequencies.

As the surface energy is increasing with the increase in ferromagnetism of the system, the total FM magnetization cannot develop monotonously. Therefore, when such surface effect overcomes the core ferromagnetism (corresponding to the doping level larger than $x = 0.18$), the magnetization of the system starts to decrease and a glass-like property is displayed.

It should be emphasized that although the FM moment is clearly observed in these nanoparticles, the antiferromagnetism is still dominant (i.e., the AFM-ordered spins in the particle cores are in the majority). Even in the $La_{0.18}Ca_{0.82}MnO_3$ nanoparticles with the largest FM moment, from the extrapolation of the M-H curve at 5 K to $H = 0$, one can get the spontaneous magnetization of $\sim$0.66 μ_B/f.u. [see Fig. 5(c), inset]. For completely FM-ordered $La_{0.18}Ca_{0.82}MnO_3$ the saturation magnetic moment should be 3.18 μ_B/f.u., so the volume of the FM phase in $La_{0.18}Ca_{0.82}MnO_3$ nanoparticles is only $\sim$20%, which basically signifies the dominant AFM phase despite the coexistence of FM clusters/shells and AFM matrix; viz. although the nanoparticles display some FM characteristics, they do not have real FM-ground state. In addition we also point out that it is not possible to distinguish the contribution from interior FM clusters and surface uncompensated spins to the observed FM moment by the magnetization measurements. We also measured the exchange-bias effect of these nanoparticles (not shown here), and the results are essentially the same as the previous reports.[12,13] But the coupling interface between the FM shell-AFM core and the coupling interface between the FM cluster-AFM core are both contributing to exchange bias, hence, it still cannot distinguish the fractions of interior FM clusters and surface FM-like spins. It should also be mentioned that although the two FM components may occur at different temperatures (FM clusters occur around T_C, whereas some surface uncompensated spins may become FM correlated at a temperature higher than T_C), the exchange-bias measurement still cannot be used to probe them because the exchange-bias effect decreases with increasing temperature and disappears

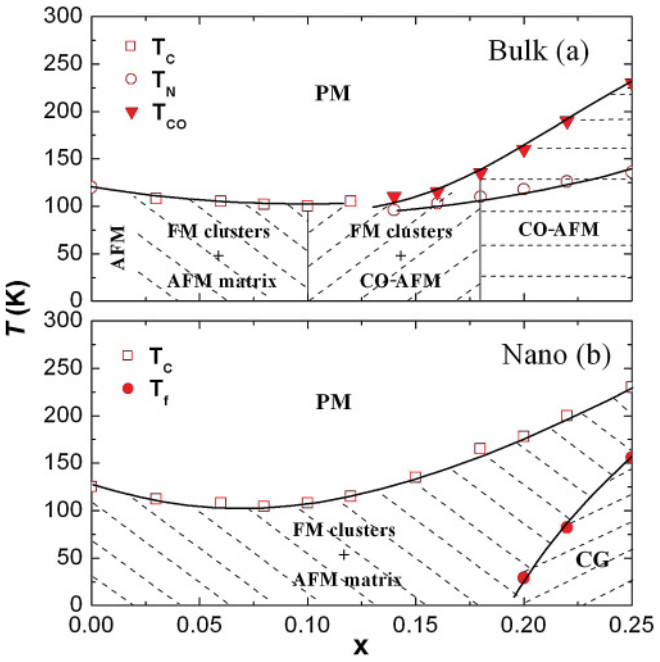

FIG. 7. (Color online) Phase diagrams for the $La_xCa_{1-x}MnO_3$ systems of (a) bulk and (b) nanoparticles. In the case of coexistence of FM clusters and AFM matrix we define the magnetic-transition temperature as T_C because of the FM characteristic in order to distinguish this region from other regions with clear CO-AFM characteristics; T_C is determined as the temperature of the negative maximum in the dM/dT curves. For the bulks, once the system turns into a CO-AFM state, we define the peak temperature in the $M(T)$ curves as CO temperature T_{CO} and the AFM transition temperature as T_N given by the bifurcation temperature of FC and ZFC $M(T)$ curves (as indicated by the arrows in Fig. 3). For the nanoparticles we define the CG-transition temperature as T_f, determined by the inflexion temperature (for $x = 0.2$) or the temperature of $dM/dT = 0$ (for $x = 0.22$ and 0.25) in the ZFC $M(T)$ curves [as indicated by the arrows in Figs. 5(d)–5(f)].

when T approaches T_C. Nonetheless, the magnetization from surface spins and other factors that affect M, such as the magnetic interactions between nanoparticles, are actually not comparable to the magnetization from FM clusters.[13,39–41] The variations in the inherent FM clusters and AFM matrix in the cores, influenced by the structural distortions and surface effect, underlie the evolution of magnetism in these nanoparticles.

On the basis of these observed magnetic variations, the phase diagrams can be established for both bulks and nanoparticles, as shown in Fig. 7. For the bulk, in a very narrow range close to $x = 0$, the system has basically an AFM-ground state. Subsequently in increasing the La content until $x = 0.1$, the system consists of FM clusters and AFM matrix; the transition temperature T_C decreases slightly. In the range of $x \sim 0.1$–0.18, although FM clusters coexist with CO-AFM matrix, the FM clusters are progressively suppressed (note that in the range of $x \sim 0.1$–0.12 no evident CO characteristic is observed, but the decrease in magnetization implies that lightly local CO may exist). When $x > 0.18$ the system becomes a homogeneous charge-ordered AFM phase. Both CO-transition temperature T_{CO} and AFM-transition temperature T_N increase. It is noticed that there are some differences between our phase diagram established by magnetic measurement and Pissas *et al.*'s[42] and Ling *et al.*'s[43] phase diagrams established by neutron diffraction. For instance for the $x = 0.1$ sample, Ling *et al.*[43] pointed out that there exists two magnetic transitions: one is the transition around 180 K from PM phase to C-AFM phase with no FM component, the other is the transition around 100 K from C-AFM phase to G-AFM phase with FM clusters. Nevertheless, the first transition can be probed only by neutron diffraction, and no changes can be observed in the temperature dependence of magnetization curve. So our magnetic measurements only reveal the second transition around 100 K (marked as T_C). Pissas *et al.*[42] and Ling *et al.*[43] also suggest a C-AFM phase with no FM component in the range from $x \sim 0.15$ to $x \sim 0.2$, but our magnetization results indicate that some weak FM clusters still exist at $x > 0.15$, and the system becomes CO-AFM at $x > 0.18$. Although Ling *et al.*,[43] Pissas *et al.*,[43] and Markovich *et al.*[45] believe that $La_{0.2}Ca_{0.8}MnO_3$ has OO but may not have CO, other studies suggest that CO or local CO more or less exist in all electron-doped $La_xCa_{1-x}MnO_3$ where $x > 0.1$.[18,22,46] In fact a literature search reveals that the reported magnetic results of an electron-doped $La_xCa_{1-x}MnO_3$ system are not quite consistent, and the intrinsic magnetic ground state of this system is still in dispute. Our magnetic-phase diagram is actually more similar to that proposed by Cheong.[46] At this stage we cannot elucidate these differences very well. But it is understandable that different measurement means work as well because different definitions might give different characteristic temperature. Moreover, as pointed out by Markovich *et al.*[11] and Belevtsev *et al.*,[47] for both bulk and nanosized manganites, extrinsic inhomogeneity that is related to various preparation methods may also modify the intrinsic physical properties. For the nanoparticles FM clusters and AFM matrix exists throughout the investigated doping range, but there is no CO; T_C first decreases slightly, reaches a minimum around $x \sim 0.08$, and then increases obviously. However, when the doping reaches $x \sim 0.2$, a re-entrant CG state is observed, and the CG-transition temperature T_f rises rapidly with x. The two-phase diagrams clearly display the different magnetic evolutions between bulks and nanoparticles.

Because of the clear ferromagnetism in the nanoparticles, we next discuss the FM class in order to better understand their magnetic interactions. As an example, Fig. 8 presents the detailed magnetic behaviors of the $La_{0.18}Ca_{0.82}MnO_3$ nanoparticles. Generally, a second-order magnetic-phase transition near T_C can be characterized by the scaling laws of spontaneous magnetization M_S and initial susceptibility χ_0 in the critical region:

$$M_S(T) = M_0 |t|^{-\beta} \tag{2}$$

at $T < T_C$,

$$\chi_0^{-1}(T) = (H/M_0) |t|^{\gamma} \tag{3}$$

at $T > T_C$, and

$$M \propto H^{1/\delta}, \tag{4}$$

at $T = T_C$, where β, γ, and δ are the critical exponents and $\delta = 1 + \gamma/\beta$. In the mean-field theory M^2 vs H/M at

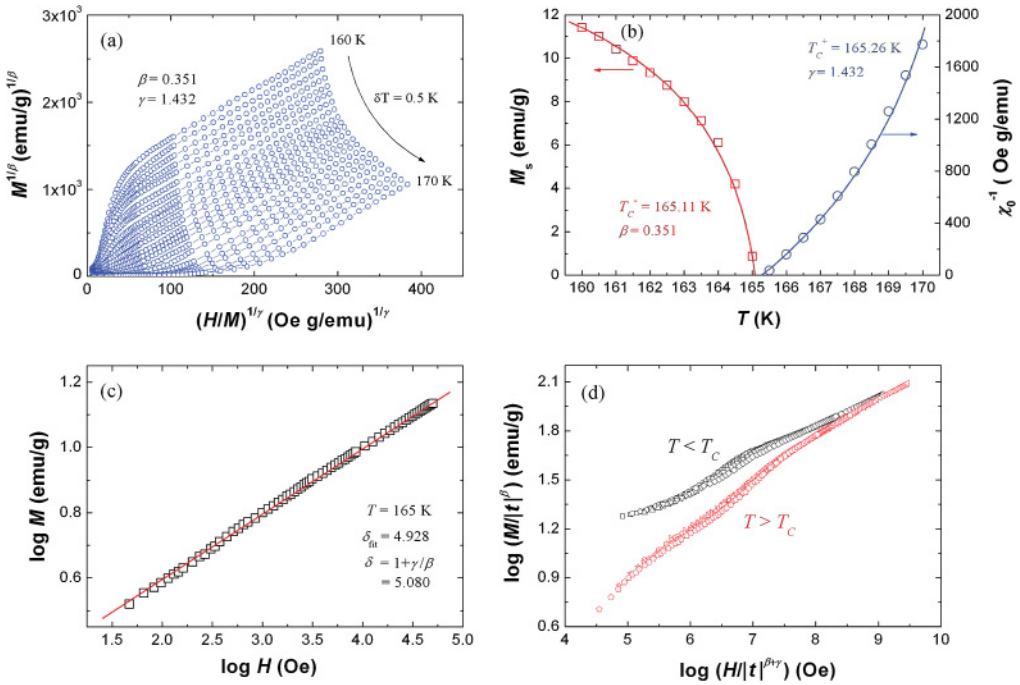

FIG. 8. (Color online) Magnetic behaviors in the $La_{0.18}Ca_{0.82}MnO_3$ nanoparticles: (a) Modified Arrott plot of $M^{1/\beta}$ vs $(H/M)^{1/\gamma}$ based on a 3D-Heisenberg model. (b) Temperature dependence of the spontaneous magnetization M_S and the inverse initial susceptibility $\chi_0{}^{-1}$ along with the fitting curves. (c) The log-log plot of the isotherm at $T = 165$ K; the solid line is the linear fitting. (d) The scaling plot of $\log(M/|t|^{\beta})$ vs $\log(H/|t|^{\beta+\delta})$ below and above T_C.

various T should give a series of parallel straight lines in the vicinity of T_C (i.e., Arrott plot). But for these nanoparticles the M^2 vs H/M curves are not linear, which suggests that the mean-field theory is not valid so the nanoparticles do not belong to the mean-field ferromagnet class. However, $M^{1/\beta}$ vs $(H/M)^{1/\gamma}$, with the critical exponents of the three-dimensional (3D) Heisenberg model, gives approximately parallel straight lines both below and above T_C [see Fig. 8(a)]. This means that the nanoparticles follow a 3D-Heisenberg class. From the plot of $M^{1/\beta}$ vs $(H/M)^{1/\gamma}$, the temperature dependences of M_S and $\chi_0{}^{-1}$ can be obtained from the extrapolation of the data at $T < T_C$ and $T > T_C$, as shown in Fig. 8(b). The fittings of M_S–T and $\chi_0{}^{-1}$–T finally give the critical exponents as $\beta = 0.351$ with $T_C^- = 165.11$ K and $\gamma = 1.432$ with $T_C^+ = 165.26$ K. Then δ is calculated to be 5.080 according to $\delta = 1 + \gamma/\beta$. Moreover, the linear fitting of the critical isotherm ($\log M$ vs $\log H$) at $T_C = 165$ K gives $\delta_{\rm fit} = 4.928$ [Fig. 8(c)]. The $\delta_{\rm fit}$ value is consistent with the calculated δ value, indicating the obtained critical exponents are reliable. A further test of the validity of this critical analysis is the scaling hypothesis

$$M(H,t) = |t|^{\beta} f_{\pm}(H/|t|^{\beta+\delta}), \tag{5}$$

where f_+ for $T > T_C$ and f_- for $T < T_C$ are regular analytical functions. Eq. (5) indicates that the plot of $M/|t|^{\beta}$ vs $H/|t|^{\beta+\delta}$ will yield two universal curves: one for $T > T_C$ and the other for $T < T_C$. As shown in Fig. 8(d), the experimental data indeed fall into two curves above and below T_C, respectively, which thus confirms that the nanoparticles belong to the 3D-Heisenberg ferromagnet class.

For a ferromagnet the class of the magnetic transition depends on the range of exchange integral $J(r)$,[48] given by $J(r) = 1/r^{d+l}$, where d is the dimension of the ferromagnet and l is the range of interaction. If $J(r)$ decreases with distance r faster than r^{-5} (viz. $l > 2$), the Heisenberg framework is valid for a 3D-isotropic ferromagnet. If $J(r)$ decreases with r slower than $r^{-4.5}$ (viz. $l < 1.5$), the mean-field framework is valid. In the intermediate range of $1.5 \leqslant l \leqslant 2$ the FM behavior belongs to different universality classes depending on l. In these nanoparticles the exchange integral $J(r)$ should decrease with distance faster than r^{-5} because the randomly distributed FM clusters are actually highly diluted by the AFM background. Because of the absence of CO, the Mn^{3+}/Mn^{4+} ions are also randomly distributed, which may weaken the cooperative spin interactions as well. This might explain the observed critical exponents of the 3D-Heisenberg model for nanoparticles. Nevertheless, it should be stressed that the magnetic correlations are complex in nanoparticles. Other lesser effects, such as the surface ferromagnetism and interactions between particles, should also be taken into account to give an entire description of the magnetic transition. Further study is needed to unambiguously answer these issues. Note that the critical exponents are slightly different from the accurate values of the 3D-Heisenberg model, which may simply result from the influence of those lesser factors.

IV. CONCLUSIONS

Magnetic properties of a series of electron-doped $La_xCa_{1-x}MnO_3$ bulks and nanoparticles in the range of $0 \leqslant x \leqslant 0.25$ have been investigated, and the magnetic-phase diagrams have been established. In the case of light doping ($0 \leqslant x \leqslant 0.1$) the magnetic properties of bulks and nanoparticles are similar,

but for heavy doping ($0.1 \leqslant x \leqslant 0.25$) the differences in magnetic evolution are clear. Although CO and antiferromagnetism gradually develop in the bulks, CO disappears in the nanoparticles, and the system exhibits an enhanced ferromagnetism. The structure refinement reveals that the conditions needed for CO to set in are not met in the nanoparticles, and the absence of CO causes a progressive development of ferromagnetism. For higher doping ($x > 0.18$) the nanoparticles display a ferromagnetism followed by a re-entrant CG state attributable to the competition between ferromagnetism and antiferromagnetism. The critical-scaling analysis indicates that the nanoparticles belong to a 3D-Heisenberg ferromagnet class, which may result from the weakening of cooperative spin interactions. These results are helpful for further understanding of the magnetic evolution in nanostructures of perovskite manganites.

[1] S. S. Rao, K. N. Anuradha, S. Sarangi, and S. V. Bhat, Appl. Phys. Lett. **87**, 182503 (2005).

[2] S. S. Rao, S. Tripathi, D. Pandey, and S. V. Bhat, Phys. Rev. B **74**, 144416 (2006).

[3] T. Sarkar, P. K. Mukhopadhyay, A. K. Raychaudhuri, and S. Banerjee, J. Appl. Phys. **101**, 124307 (2007).

[4] T. Sarkar, B. Ghosh, A. K. Raychaudhuri, and T. Chatterji, Phys. Rev. B **77**, 235112 (2008).

[5] T. Zhang and M. Dressel, Phys. Rev. B **80**, 014435 (2009).

[6] Z. Jirák, E. Hadová, O. Kaman, K. Knížek, M. Maryško, E. Pollert, M. Dlouhá, and S. Vratislav, Phys. Rev. B **81**, 024403 (2010).

[7] C. L. Lu, S. Dong, K. F. Wang, F. Gao, P. L. Li, L. Y. Lv, and J. M. Liu, Appl. Phys. Lett. **91**, 032502 (2007).

[8] K. S. Shankar, S. Kar, A. K. Raychaudhuri, and G. N. Subbanna, Appl. Phys. Lett. **84**, 993 (2004).

[9] V. Markovich, I. Fita, A. Wisniewski, G. Jung, D. Mogilyansky, R. Puzniak, L. Titelman, and G. Gorodetsky, Phys. Rev. B **81**, 134440 (2010).

[10] P. Chai, X. Y. Wang, S. Hu, X. J. Liu, Y. Liu, M. F. Lv, G. S. Li, and J. Meng, J. Phys. Chem. C **113**, 15817 (2009).

[11] V. Markovich, I. Fita, A. Wisniewski, D. Mogilyansky, R. Puzniak, L. Titelman, and G. Gorodetsky, J. Appl. Phys. **108**, 063918 (2010).

[12] X. H. Huang, J. F. Ding, G. Q. Zhang, Y. Hou, Y. P. Yao, and X. G. Li, Phys. Rev. B **78**, 224408 (2008).

[13] V. Markovich, I. Fita, A. Wisniewski, D. Mogilyansky, R. Puzniak, L. Titelman, C. Martin, and G. Gorodetsky, Phys. Rev. B **81**, 094428 (2010).

[14] T. Zhang, T. F. Zhou, T. Qian, and X. G. Li, Phys. Rev. B **76**, 174415 (2007).

[15] E. Rozenberg, M. Auslender, A. I. Shames, D. Mogilyansky, I. Felner, E. Sominskii, A. Gedanken, and Y. M. Mukovskii, Phys. Rev. B **78**, 052405 (2008).

[16] S. Dong, F. Gao, Z. Q. Wang, J. M. Liu, and Z. F. Ren, Appl. Phys. Lett. **90**, 082508 (2007).

[17] S. Dong, R. Yu, S. Yunoki, J. M. Liu, and E. Dagotto, Phys. Rev. B **78**, 064414 (2008).

[18] A. Maignan, C. Martin, F. Damay, and B. Raveau, Chem. Mater. **10**, 950 (1998); B. Raveau, A. Maignan, C. Martin, and M. Hervieu, *ibid.* **10**, 2641 (1998).

[19] M. B. Salamon and M. Jaime, Rev. Mod. Phys. **73**, 583 (2001).

[20] P. K. Siwach, H. K. Singh, and O. N. Srivastava, J. Phys. Condens. Matter **20**, 273201 (2008).

[21] *Colossal Magnetoresistance, Charge Ordering and Related Properties of Manganese Oxides*, edited by C. N. R. Rao and B. Raveau (World Scientific, Singapore, 1998).

[22] L. Sudheendra, A. R. Raju, and C. N. R. Rao, J. Phys. Condens. Matter **15**, 895 (2003); Y. Wang, Y. Sui, X. J. Wang, and W. H. Su, *ibid.* **21**, 196004 (2009).

[23] M. Respaud, J. M. Broto, H. Rakoto, J. Vanacken, P. Wagner, C. Martin, A. Maignan, and B. Raveau, Phys. Rev. B **63**, 144426 (2001).

[24] C. Kapusta, P. C. Riedi, M. Sikora, and M. R. Ibarra, Phys. Rev. Lett. **84**, 4216 (2000).

[25] Y. Wang, Y. Sui, H. J. Fan, X. J. Wang, Y. T. Su, W. H. Su, and X. Y. Liu, Chem. Mater. **21**, 4653 (2009).

[26] M. Abbate, F. M. F. de Groot, J. C. Fuggle, A. Fujimori, O. Strebel, F. Lopez, M. Domke, G. Kaindl, G. A. Sawatzky, M. Takano, Y. Takeda, H. Eisaki, and S. Uchida, Phys. Rev. B **46**, 4511 (1992); M. Sirena, N. Haberkorn, M. Granada, L. B. Steren, and J. Guimpel, J. Appl. Phys. **105**, 033902 (2009).

[27] Y. Wang, Y. Sui, X. J. Wang, Y. T. Su, W. H. Su, X. Y. Liu, and H. J. Fan, J. Phys. Chem. C **114**, 1491 (2010).

[28] E. O. Wollan and W. C. Koehler, Phys. Rev. **100**, 545 (1955).

[29] R. N. Bhowmik, R. Nagarajan, and R. Ranganathan, Phys. Rev. B **69**, 054430 (2004).

[30] P. G. Radaelli, D. E. Cox, M. Marezio, and S. W. Cheong, Phys. Rev. B **55**, 3015 (1997).

[31] Z. Jirak, F. Damay, M. Hervieu, C. Martin, B. Raveau, G. Andre, and F. Bouree, Phys. Rev. B **61**, 1181 (2000).

[32] F. Millange, S. de Brion, and G. Chouteau, Phys. Rev. B **62**, 5619 (2000).

[33] Although Markovich *et al.* emphasize that the compound $La_{0.2}Ca_{0.8}MnO_3$ displays OO but no CO (Ref. 13), many literatures have pointed out that there exist CO or local CO more or less in all electron-doped $La_xCa_{1-x}MnO_3$ with $x > 0.1$ (Refs. 18, 22 and 46). So herein we do not try to prove the existence of CO and do not strictly distinguish CO and OO in $La_xCa_{1-x}MnO_3$ bulks; instead, we just follow the previous proposal that CO exists in all $La_xCa_{1-x}MnO_3$ bulks with $x > 0.1$, and generally attribute the peak in the *M-T* curves to CO.

[34] Y. Wang and H. J. Fan, Appl. Phys. Lett. **98**, 142502 (2011).

[35] Y. Wang, Y. Sui, X. J. Wang, W. H. Su, and X. Y. Liu, J. Appl. Phys. **108**, 063928 (2010).

[36] M. J. Benitez, O. Petracic, E. L. Salabas, F. Radu, H. Tüysüz, F. Schüth, and H. Zabel, Phys. Rev. Lett. **101**, 097206 (2008).

[37] T. Zhu, B. G. Shen, J. R. Sun, H. W. Zhao, and W. S. Zhan, Appl. Phys. Lett. **78**, 3863 (2001).

[38] P. Dey and T. K. Nath, Phys. Rev. B **73**, 214425 (2006).

[39] C. R. H. Bahl, M. F. Hansen, T. Pedersen, S. Saadi, K. H. Nielsen, B. Lebech, and S. Mørup, J. Phys. Condens. Matter **18**, 4161 (2006); S. Mørup, D. E. Madsen, C. Frandsen, C. R. H. Bahl, and M. F. Hansen, *ibid.* **19**, 213202 (2007).

[40]J. Nogués, V. Skumryev, J. Sort, S. Stoyanov, and D. Givord, Phys. Rev. Lett. **97**, 157203 (2006).
[41]M. F. Hansen, C. B. Koch, and S. Mørup, Phys. Rev. B **62**, 1124 (2000).
[42]M. Pissas and G. Kallias, Phys. Rev. B **68**, 134414 (2003).
[43]C. D. Ling, E. Granado, J. J. Neumeier, J. W. Lynn, and D. N. Argyriou, Phys. Rev. B **68**, 134439 (2003).
[44]M. Pissas, G. Kallias, M. Hofmann, and D. M. Többens, Phys. Rev. B **65**, 064413 (2002).
[45]V. Markovich, I. Fita, R. Puzniak, E. Rozenberg, C. Martin, A. Wisniewski, Y. Yuzhelevski, and G. Gorodetsky, Phys. Rev. B **71**, 134427 (2005).
[46]S. W. Cheong, *Colossal Magnetoresistance Oxides* (Gordon & Breach, London, 1999).
[47]B. I. Belevtsev, D. G. Naugle, K. D. D. Rathnayaka, A. Parasiris, and J. F. Finowicki, Physica B **355**, 341 (2005).
[48]M. E. Fisher, S. K. Ma, and B. G. Nickel, Phys. Rev. Lett. **29**, 917 (1972).